A VORTEX PANEL METHOD FOR THE SOLUTION OF INCOMPRESSIBLE UNSTEADY FLOW

89-1284-CP

Rokhsaz, K.[+], Selberg, B. P.[#], and Eversman, W.[@]

Department of Mechanical and Aerospace Engineering
University of Missouri-Rolla, Rolla, MO 65401

ABSTRACT

A vortex panel method is presented for the solution of incompressible unsteady aerodynamic problems for lifting surfaces with finite thickness. The accuracy and robustness of the method is demonstrated through comparisons with the existing numerical data and independent test cases. Also, through numerous examples, the flexibility of this method in handling different types trailing edge shapes and multiple interfering geometries is shown.

Furthermore, the method is used to analyze the effects of airfoil thickness on aerodynamic coefficients of multi-element lifting systems. It is shown that although the influence of thickness is negligible for single element airfoils, it can be profound for closely coupled airfoils and slotted flaps.

NOMENCLATURE

C	reference chord length
$C_{l\alpha}$	lift coefficient per A.O.A.
$C_{m\alpha}$	pitching moment coefficient per A.O.A.
C_p	pressure coefficient
C_{ps}	steady state part of pressure coefficient
C_{pu}	unsteady part of pressure coefficient
$\vec{e}_s$	unit vector parallel to the surface
G	non-dimensional gap
h	displacement in plunge
h_o	amplitude of displacement in plunge
$\vec{n}$	unit vector normal to the surface
n_i	amplitude of the unsteady part of $\vec{n}$
n_s	steady state part of the unit normal vector
n_u	unsteady part of the unit normal vector
p	pressure
p_∞	pressure in free stream flow
r	radius vector
s	coordinate parallel the surface or the wake
S	hyper-surface defining the airfoil
S_i	amplitude of the unsteady part of S
S_s	steady state part of S
S_u	unsteady part of S
t	time
V_∞	free stream velocity
V_s	steady state velocity tangent to the wake
x	Cartesian x axis
z	Cartesian z axis
α	angle of attack
$\bar{\alpha}$	steady state angle of attack
α_o	amplitude of the unsteady angle of attack
γ	local unsteady vorticity
$\bar{\gamma}$	amplitude of local vorticity
Δ	difference between upper and lower sides
$\vec{\nabla}$	gradient operator
∇^2	Laplacian operator
θ	potential of a unit vortex
ξ	coordinate tangent to the wake
ρ	air density
Φ	total velocity potential
ϕ_∞	velocity potential of the free stream flow
ϕ_s	steady state perturbation velocity potential
ϕ_u	unsteady perturbation velocity potential
ψ	amplitude of unsteady perturbation potential
ω	circular frequency
$\bar{\omega}$	reduced frequency, $C\,\omega/2\,V_\infty$

+ Teaching Fellow in Aerospace Engineering, Senior Member of AIAA.
# Professor and Associate Chairman of Aerospace Engineering, Associate Fellow of AIAA.
@ Curators' Professor of Mechanical and Aerospace Engineering, Associate Fellow of AIAA.

I. INTRODUCTION

Airfoils undergoing oscillatory motion, can demonstrate aerodynamic characteristics which are substantially different from their steady state behavior. The most profound of these is the phase difference between the motion and the generation of aerodynamic forces and moments. Accurate prediction of these forces and their phase angles is of major importance in flutter analysis where airfoils are assumed to move harmonically with very small amplitudes. Any inaccuracies in aerodynamic calculations can lead to errors in evaluating the flutter speed. Steady state aerodynamic behavior of closely coupled airfoils in two dimensional incompressible flow was studied in references 1 and 2. It was demonstrated that although the influence of thickness is not very critical in the case of a single airfoil, it can be profound for closely coupled lifting surfaces. The same behavior is logically expected to be present for harmonically oscillating airfoils. However, the present state of the art in predicting such effects appears to be rather poor. The thin airfoil formulations, which are computationally fast, do not account for the effects of thickness, camber, and non-zero mean incidence angles. On the other hand, the current methods capable of doing so, appear to be more of a novelty nature because of their inapplicability. They either require exorbitant amounts of computation time or they include unacceptable numerical instabilities. Both of these characteristics exclude the use of these methods for flutter analysis where multiple solutions have to be performed accurately and rapidly over a wide range of frequencies. Considering the above limitations, in order to study the effect of thickness on closely coupled airfoils, a fast and robust solution method has to be developed. It is the intention of this document to demonstrate such a technique and its application to interfering lifting surfaces. Furthermore, it is intended to demonstrate the effects of thickness on the aerodynamic and dynamic characteristics of closely coupled airfoils.

II. REVIEW OF LITERATURE

The bulk of research in the recent years has been concerned with compressible and transonic problems. A variety of numerical and analytical solutions have been developed in these areas. Nevertheless, many a question remain ambiguous regarding incompressible solutions. These techniques can be divided into two major categories: 1) analytical methods, and 2) numerical approaches. What follows is a brief review of the current techniques for incompressbile flow solutions.

A. ANALYTICAL METHODS

Analytical solutions date back to that of Theodorsen (3). His formulation of the problem resembles the thin airfoil theory used in steady state aerodynamics. The airfoil is replaced by its chord line at zero mean incidence angle with respect to the upstream flow. Effects of camber, thickness, and non-zero angles of attack are totally ignored in this formulation. The wake is assumed to be a flat vortex sheet with uniform steady state velocity equal to that of the upstream flow. Although this method is applicable to single airfoil cases only, it can accommodate a plain flap through the proper application of the boundary conditions. Like all thin airfoil formulations, this technique results in the difference between the pressures over the upper and lower surfaces of the airfoil.

The first analytical technique including the effects of thickness, was developed by Hewsone-Browne (4). A similar formulation of the problem was also presented by van de Vooren and van de Vel (5). These approaches make extensive use of conformal mapping and are only applicable to special classes of airfoils which lend themselves to simple transformations. In both methods, a sinlge symmetric airfoil is placed at zero mean incidence angle and then conformally mapped into a circle. The wake is assumed to be a flat vortex sheet emanating from the trailing edge. However, unlike the previous method, the exact steady state velocity distribution is used over the wake. For these analytical solutions to become mathematically feasible, the airfoil shape must be transformed into a circle in a simple single step operation. Although the latter method results in the exact pressure distribution, it cannot accommodate flaps, camber, general airfoil shapes, or non-zero mean incidence angles. Furthermore, considering the complexity of transformation of multiple airfoils into circles, these approaches appear to be totally inapplicable to interfering lifting surfaces.

B. NUMERICAL METHODS

Numerical methods can be placed into two general categories: 1) finite difference methods and 2) surface singularity techniques.

Finite difference solutions have the advantage of being able to accommodate nonlinearities very easily. In these methods, the problem is formulated in terms of disturbance velocity potential. The governing equations are simply discretized regardless of the nature of nonlinearities, and solved using any of a number of iterative techniques. However, interference of the wake surface with the grid system can pose a rather formidable numerical problem. In order to alleviate these problems, adaptive mesh generation has to be employed, at the cost of regenerating the entire grid system for each iteration cycle. Also, in this approach, the application of the Kutta condition, which is expressed in terms of the pressure, can produce difficulties. Furthermore, since the problem is formulated in terms of the disturbance velocity potential, the grid system has to extend far enough into the solution domain for this variable to vanish. At the same time, in order to achieve an accurate pressure distribution, a very large number of points must be employed on the surface of the airfoil. Considering the above factors, these approaches require very large amounts of computer storage and/or computation time. This can be a very strong drawback to their use for flutter analysis where multiple solutions over a wide range of frequencies have to be performed quickly. It should be mentioned that any finite element formulation also suffers from the same handicaps, perhaps with the exception of the required number of points on the surfaces. However, like the last analytical method discussed, both approaches result in the actual pressure distribution over the surfaces.

Surface singularity or boundary element methods are based on two different approaches; acceleration potential, and velocity potential formulations. In the acceleration potential method, the problem is formulated in terms of the difference in pressures of the lower and the upper surfaces, using Euler's equation. The resulting integral equation spans over the leading edge stagnation streamline as well as over the airfoil. However, the integral equation vanishes on the wake in accordance with the Kutta condition. This approach was first introduced by Possio (6) for the fully linearized compressible subsonic problem. Grzedzinski (7) adopted this method for analyzing the interference problem in incompressible flow over biplanes. This solution also ignores all non-linearities including the effects of thickness.

The first set of boundary element formulations including the effects of thickness in the literature are due to Giesing (8,9,10). Here, the problem is again formulated in terms of the perturbation velocity potential. The airfoil is modeled by source panels of linearly varying strength and a constant strength vortex panel. This method strongly resembles that of Hess (11) for the steady state problem. In the nonlinear form, the airfoil is allowed to undergo small displacements over small increments of time, during which a steady state solution is performed. The shed vorticity is modeled by point vortices. During each time step, new perturbation velocities and new locations for these point vortices are calculated. The linearized formulation of the problem is derived from the nonlinear formulation. In this case, the governing matrices are expanded in series with their higher order terms neglected. In either case, these techniques suffer from strong numerical instabilities, specially for airfoils with cusped trailing edges, as discussed by Hess (12). Furthermore, the nonlinear solution requires exorbitant amounts of computation time for harmonically oscillating airfoils. A complete steady state solution has to be carried out for each time step (i.e. for each descrete wake vortex). The enormity of the required computation time becomes evident considering that thousands of descrete vortices are required to achieve a converged solution. However, since these methods are posed in terms of the velocity potential, they yield the actual pressure

distribution on the surfaces. Also, since they do not require a grid system surrounding the airfoils, their application to multiple interfering airfoils is quite simple.

Another surface singularity method has been proposed by Hounjet (13). Although he uses the method to solve the subsonic flow problem, linearized in Mach number, his method should also be easily applicable to incompressible cases as well. This method employs doublet panels of piecewise continuous strength. The weakness of this approach lies in the fact that with doublet panels, the distribution of the velocity potential over the surface has the same interpolation order as that of the doublet strength, as explained by Banerjee and Butterfield (14), that is a piecewise linear distribution of the velocity, requires the use of quadratic distribution of doublets. This severely complicates the task of resolving the singularities over the surface. On the other hand, linear distribution of doublets over the surface results in discontinuities in the velocity over the surface, and therefore numerical instabilities with coarse grids. In order to alleviate this problem, a very large number of points must be employed over the surface which in turn increases the required computation time.

III. FORMULATION

A. THE AERODYNAMIC MODEL

1. Governing Equation. As demonstrated by Keuthe and Chow (15), expressing the continuity equation in terms of the velocity potential for an irrotational incompressible flow results in

$$\nabla^2\Phi = 0. \tag{1}$$

Dividing the velocity potential into three components

$$\Phi = \phi_\infty + \phi_s + \phi_u \tag{2}$$

equation 1 can be written as

$$\nabla^2\phi_s = 0, \tag{3}$$

$$\nabla^2\phi_u = 0. \tag{4}$$

which are the equations of motion for steady and unsteady flows, respectively.

2. Boundary Conditions. Boundary conditions related to equation 1 are

$$\Phi(r \to \infty) = \phi_\infty, \tag{5}$$

$$\frac{DS}{Dt} = 0. \tag{6}$$

Introducing equation 2 into these equations, equation 5 results in

$$\phi_s(r \to \infty) = 0, \tag{7}$$

$$\phi_u(r \to \infty) = 0. \tag{8}$$

For the flow tangency condition one can let

$$\vec{V} = \vec{\nabla}\phi_\infty + \vec{\nabla}\phi_s + \vec{\nabla}\phi_u$$

and then since

$$\frac{DS}{Dt} = \frac{\partial S}{\partial t} + \vec{V}\cdot\vec{\nabla}S = \frac{\partial S_u}{\partial t} + \vec{V}\cdot(\vec{\nabla}S_s + \vec{\nabla}S_u)$$

hence

$$\frac{1}{|\vec{\nabla}S|}\left(\frac{\partial S_u}{\partial t}\right) + \vec{V}\cdot(\vec{n}_s + \vec{n}_u) = 0.$$

where

$$\vec{n} = \vec{n}_s + \vec{n}_u = \frac{\vec{\nabla}S_s}{|\vec{\nabla}S|} + \frac{\vec{\nabla}S_u}{|\vec{\nabla}S|}$$

is the unit vector normal to the surface. Therefore equation 6 becomes

$$\frac{1}{|\vec{\nabla}S|}\left(\frac{\partial S_u}{\partial t}\right) + (\vec{\nabla}\phi_\infty + \vec{\nabla}\phi_s + \vec{\nabla}\phi_u)\cdot\vec{n}_s + (\vec{\nabla}\phi_\infty + \vec{\nabla}\phi_s)\cdot\vec{n}_u + \vec{\nabla}\phi_u\cdot\vec{n}_u = 0.$$

Since this must hold at every instant of time, then

$$(\vec{\nabla}\phi_\infty + \vec{\nabla}\phi_s)\cdot\vec{n}_s = 0 \tag{9}$$

which is the steady boundary condition, and

$$\frac{1}{|\vec{\nabla}S|}\left(\frac{\partial S_u}{\partial t}\right) + \vec{\nabla}\phi_u\cdot\vec{n}_s + (\vec{\nabla}\phi_\infty + \vec{\nabla}\phi_s)\cdot\vec{n}_u + \vec{\nabla}\phi_u\cdot\vec{n}_u = 0 \tag{10}$$

for the unsteady motion.

3. Pressure Coefficient. For the origin moving with constant speed, V_∞, from Bernoulli's equation

$$\frac{\partial\Phi}{\partial t} + \frac{1}{2}\vec{\nabla}\Phi\cdot\vec{\nabla}\Phi + \frac{p}{\rho} = \frac{p_\infty}{\rho} + \frac{1}{2}V_\infty^2$$

Applying equation 2 , expanding, and rearranging this results in

$$C_p = C_{ps} + C_{pu}$$

$$= \frac{2(p - p_\infty)}{\rho V_\infty^2} = [1 - \frac{(\vec{\nabla}\phi_\infty + \vec{\nabla}\phi_s)^2}{V_\infty^2}] \qquad (11)$$

$$- \frac{2}{V_\infty^2} [\frac{\partial \phi_u}{\partial t} + (\vec{\nabla}\phi_\infty + \vec{\nabla}\phi_s) \cdot \vec{\nabla}\phi_u + \vec{\nabla}\phi_u \cdot \vec{\nabla}\phi_u]$$

4. Kutta Condition. At the trailing edge and over the wake surface, the difference in pressure between the upper and lower surfaces must vanish. From equation 11 , this implies for steady state flow

$$\Delta[\,(\vec{\nabla}\phi_\infty + \vec{\nabla}\phi_s)^2\,] = 0. \qquad (12)$$

and for unsteady flow

$$\Delta[\,(\vec{\nabla}\phi_\infty + \vec{\nabla}\phi_s + \vec{\nabla}\phi_u) \cdot \vec{\nabla}\phi_u + \frac{\partial \phi_u}{\partial t}\,] = 0. \qquad (13)$$

It should be mentioned that equation 12 is the standard Kutta condition employed in many steady state solutions. This equation can be replaced by zero circulation condition for non-lifting problems.

5. Harmonic Motion With Small Amplitude. Since in incompressible flow waves propagate with infinite speed, the dependence of the velocity potential on time will have the same form as the motion of the surface. This implies that

$$\phi_u = \psi \alpha_o e^{i\omega t}, \quad S_u = S_i \alpha_o e^{i\omega t}, \quad \text{and} \quad \vec{n}_u = \vec{n}_i \alpha_o e^{i\omega t}$$

where α_o is the amplitude of motion in pitch. Here, this amplitude is assumed to be very small compared to other dimensions in the problem. For plunging motion, α_o can be replaced by $(2h/C)$. Then for the unsteady problem, equation 4 in terms of ψ , becomes

$$\nabla^2 \psi = 0. \qquad (14)$$

subject to the boundary conditions

$$\psi(r \to \infty) = 0, \qquad (15)$$

$$\vec{\nabla}\psi \cdot \vec{n}_s = - \frac{i\omega S_i}{|\vec{\nabla} S|} + (\vec{\nabla}\phi_\infty + \vec{\nabla}\phi_s) \cdot \vec{n}_i. \qquad (16)$$

Equation 16 is the same as equation 10 with the last term ignored due to its higher order in terms of α_o. Likewise, ignoring the higher order term of equation 11 , the expression for pressure coefficient becomes,

$$C_{pu} = - \frac{2\alpha_o e^{i\omega t}}{V_\infty^2} [(\vec{\nabla}\phi_\infty + \vec{\nabla}\phi_s) \cdot \vec{\nabla}\phi_u + i\omega\psi] \qquad (17)$$

For Kutta condition, after eliminating the higher order term, equation 13 can be written as

$$\Delta[\,(\vec{\nabla}\phi_\infty + \vec{\nabla}\phi_s) \cdot \vec{\nabla}\phi_u + \frac{\partial \phi_u}{\partial t}\,] = 0. \qquad (18)$$

Since the wake is assumed to be the steady state trailing edge stream line, we can define ξ to be the coordinate parallel to the wake and write equation 18 as

$$\Delta[\, V_s(\xi) \frac{\partial \phi_u}{\partial \xi} + \frac{\partial \phi_u}{\partial t}\,] = 0. \qquad (19)$$

Then on the wake surface

$$V_s(\xi) \frac{\partial}{\partial \xi} [\,\phi_u^+ - \phi_u^-\,] + \frac{\partial}{\partial t} [\,\phi_u^+ - \phi_u^-\,] = 0. \qquad (20)$$

where + and - refer to above and below the wake surface, respectively. Now if the wake surface is to be represented by a vortex sheet, the above equation is equivalent to

$$V_s(\xi)\gamma(\xi, t) + \frac{\partial}{\partial t} (\,\phi_u^+ - \phi_u^-\,) = 0.$$

Differentiating with respect to ξ ,

$$\frac{\partial}{\partial \xi} [\, V_s(\xi)\gamma(\xi, t)\,] + \frac{\partial}{\partial t} \gamma(\xi, t) = 0. \qquad (21)$$

Now in accordance with the definition of the unsteady velocity potential, we let

$$\gamma(\xi, t) = \bar{\gamma}(\xi)\alpha_o e^{i\omega t}$$

Therefore, equation 21 becomes

$$\frac{d}{d\xi} [\, V_s(\xi)\bar{\gamma}(\xi)\,] + i\omega\bar{\gamma}(\xi) = 0.$$

Integrating from the trailing edge on along the wake results in

$$\bar{\gamma}(\xi) = \frac{[\,\bar{\gamma}(\xi) V_s(\xi)\,]_{TE}}{V_s(\xi)} \exp[\, - i\omega \int_{TE}^{\xi} \frac{d\zeta}{V_s(\zeta)}\,] \qquad (22)$$

where on the airfoil trailing edge

$$\bar{\gamma}(\xi)_{TE} = [\,\bar{\gamma}(\xi)^+ + \bar{\gamma}(\xi)^-\,]_{TE}.$$

6. Discussion of the Equations. A simple examination of this formulation reveals that the problem is governed by an elliptic differential equation, subject entirely to Neumann boundary conditions. Therefore, a unique solution for the velocity potential can be obtained only in the presence of some constraint. However, in both steady and unsteady cases, the uniqueness conditions

imposed on the problem, are also of the Neumann type. In steady state cases, this does not pose a serious problem, for the fact that the value of the velocity potential itself is inconsequential. The pressure is entirely a function of the local velocity which can be determined uniquely, as long as the velocity potential is unique to within a constant. In unsteady cases, however, the unsteady perturbation potential appears in the expression for pressure coefficient. Therefore, pressure coefficient, much like the velocity potential, can be determined uniquely, only to within a constant. This still allows correct imposition of the Kutta condition because again this condition is expressed in terms of the difference in the pressures of the upper and the lower sides of the wake. Likewise, lift and pitching moment coefficients, being functions of the difference in pressures, can be determined uniquely.

7. Discretization and Numerical Solution. The details of discretization and the numerical solution are presented in reference 16. However, a brief outline of the method will be presented here.

The airfoil is broken into a polygon with an arbitrary number of sides and a control point at the center of each panel. A vortex sheet with linear variation of vorticity is placed on each panel. The steady state solution is obtained using the method of Stevens et al (17). However, the steady state Kutta condition of reference 17 is replaced by equation 12, applied to the last two panels immediately above and below the trailing edge. This form of the Kutta condition is numerically more accurate and stable than the condition of vanishing vorticity at the trailing edge, proposed by Stevens et al. Furthermore, this represents a more general form of the Kutta condition, for it is also applicable to airfoils which have a finite trailing edge angle. Also, application of the Kutta condition in any form results in an overdetermined system of equations. In order to alleviate this problem, the flow tangency condition on the trailing edge panel normal to the chord can be ignored, if the airfoil has a finite trailing edge thickness. For sections with a sharp trailing edge, a finite thickness in the order of 0.001% of the chord length can be introduced at this point.

Once the steady state solution is obtained, the location of, and the velocity distribution on, the trailing edge streamline can be determined by a shooting technique. In the unsteady solution, this streamline is assumed to form the wake.

A similar logic is followed for the unsteady solution. However, in this case, the wake is also modeled by vortex panels of linearly varying strength. The amplitude of the unsteady perturbation potentaial, from the superposition principle is then given by;

$$2\pi\psi(x,z) = -\sum_{j=1}^{N}\int_{l_j}\bar{\gamma}_j(s)\theta\, ds - \int_{TE}^{\infty}\bar{\gamma}(s)\theta\, ds + \bar{C}, \quad (23)$$

where $\bar{\gamma}_j(s)$ and $\bar{C}$ are the linear variation of vorticity along each panel and the constant of integration, respectively. Applying the flow tangency condition,

$$2\pi\vec{\nabla}\psi(x,z)\cdot\vec{n}_s = -\sum_{j=1}^{N}\int_{l_j}\bar{\gamma}_j(s)\vec{\nabla}\theta\cdot\vec{n}_s\, ds - \int_{TE}^{\infty}\bar{\gamma}(s)\vec{\nabla}\theta\cdot\vec{n}_s\, ds \quad (24)$$

As demonstrated by Moran (18), this leads to linear variation of the velocity on each panel, therefore, implying a quadratic distribution of the velocity potential. The local strength of the vortex sheet is related, through the Kutta condition, to the sum of the vortices at the two corners of the trailing edge, through equation 22 . This model of the wake is used to a distance of ten chord lengths behind the trailing edge. Past this point, the wake curvature becomes negligible so the wake is assumed to be flat with constant steady state velocity. The panel sizes are increased to ten percent of the vorticity wavelength, and integrations for velocity potential and its gradient are carried out to another one hundred and fifty chord lengths. This length was determined to be necessary for satisfactory convergence of the lift and the pitching moment coefficients. Also, assuming a flat wake past a certain distance behind the trailing edge, results in a closed form solution for the total vorticity over that part of the wake. This total vorticity has to be fixed in order to satisfy the Kelvin's theorem, or

$$\int_{airfoil}\bar{\gamma}(s)\, ds + \int_{wake}\bar{\gamma}(s)\, ds = CONSTANT \quad (25)$$

For convenience, this constant can be set to zero.

Once the unsteady vortex strengths are determined, the unsteady velocity distribution can be calculated from

$$2\pi\vec{\nabla}\psi(x,z)\cdot\vec{e}_s = -\pi\bar{\gamma} - \sum_{j=1}^{N}\int_{l_j}\bar{\gamma}_j(s)\vec{\nabla}\theta\cdot\vec{e}_s\, ds - \int_{TE}^{\infty}\bar{\gamma}(s)\vec{\nabla}\theta\cdot\vec{e}_s\, ds \quad (26)$$

In order to find the unsteady velocity potential, the value of this parameter is assumed to be zero on one side of the trailing edge. Then a simple line integration of the velocity tangent to the surface results in the value of the velocity potential, unique to within a constant, as discussed in the previous section. For symmetric airfoils, undergoing harmonic motion about a zero mean incidence angle, this constant can be determined from the pressure coefficient. In these cases, the pressure is an odd function with respect to the chord line. At the same time, from the Kutta condition, the difference between the upper and lower surface pressures must vanish at the trailing edge. This leads to the conclusion that in such cases, the pressure coefficient itself must vanish at this point and allows exact calculation of this parameter everywhere over the surface.

IV. RESULTS AND DISCUSSION

A. AERODYNAMIC SOLUTION

1. Single Element Unsteady Solution. The first airfoil studied using this method was that of reference 5. Figure 1 shows the comparison between the analytical and vortex panel results. The airfoil is symmetric, approximately 14% thick, and has a finite trailing edge angle. The vortex panel results were obtained with 71 panels. As demonstrated by this figure, excellent agreement between the two sets of results is present everywhere except in the real part near the leading edge. The minor disagreements in this region are due to lack of sufficient number points there. In this case, due to the symmetry of the airfoil, the constant of integration for the velocity potential could be explicitly evaluated, resulting in exact distribution of the pressure coefficient. Figure 2

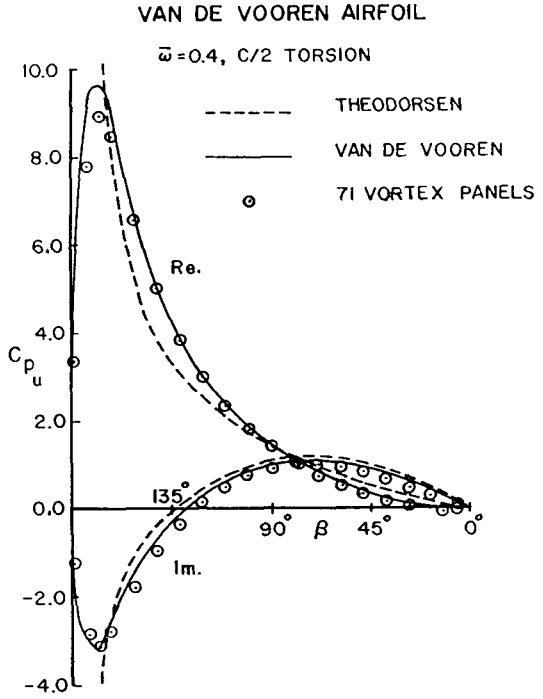

Figure 1. Unsteady pressure distribution on the van de Vooren airfoil.

shows the same type of comparison for a 25.5% thick Joukowski section, used in references 8 through 10. The vortex panels results were obtained with 57 panels. Again, there is excellent agreement among the three sets of results. However, a total absence of any oscillations in the pressure coefficient, as predicted by the vortex panel method, is clearly evident near the trailing edge. This is due solely to the greater accuracy of this method. In fact, in references 8 through 10, the trailing edge shape had to be modified in order to minimize these oscillations. The 25.5% thick Joukowski airfoil was also used as the subject of a convergence test. The results for 49 panels differed from the results for 199 panels by a maximum of only 7% in the imaginary part of the lift-curve slope.

Figures 3 through 6 show the effects of thickness on the aerodynamic coefficients over a wide range of reduced frequencies. The numerical results in these figures were all obtained with 71 vortex panels. Here, the trends are

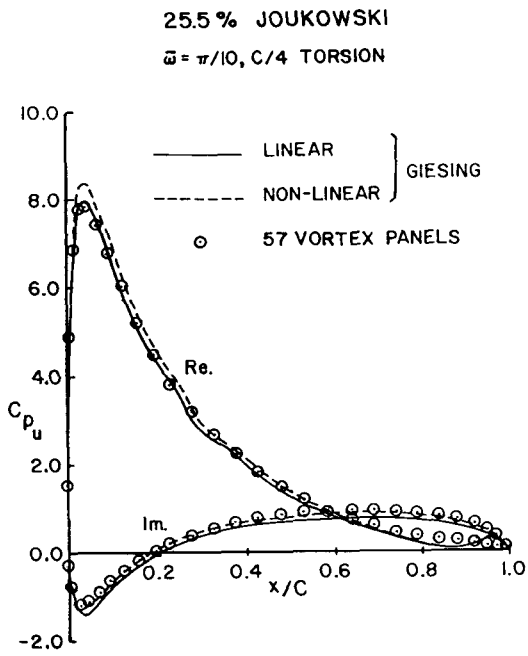

Figure 2. Unsteady pressure distribution on a 25.5% Joukowski airfoil.

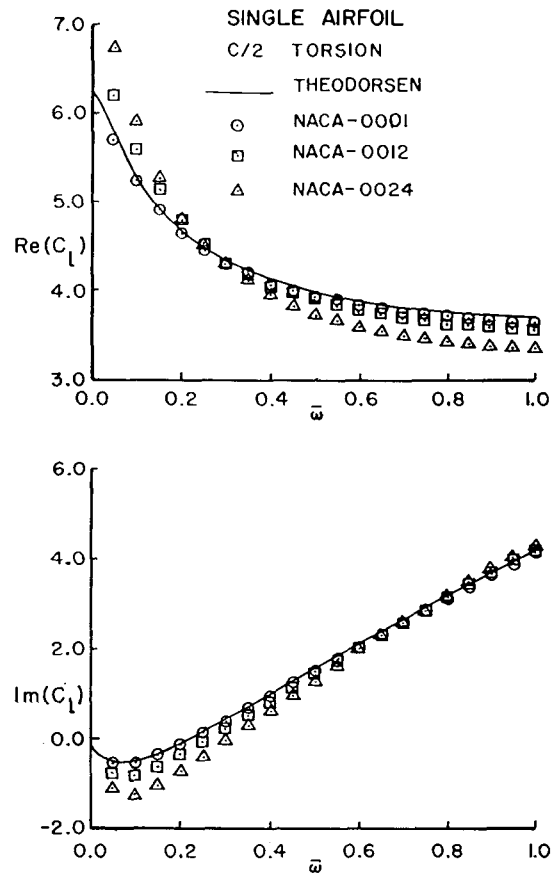

Figure 3. Effect of thickness on unsteady lift coefficient.

very much in agreement with those of reference 4. While the lift coefficient does not appear to be too sensitive to thickness, the pitching moment coefficient shows quite a different behavior. At the higher values of the reduced frequency, differences as large as 40% are present in the pitching moment coefficient. This can lead to substantial

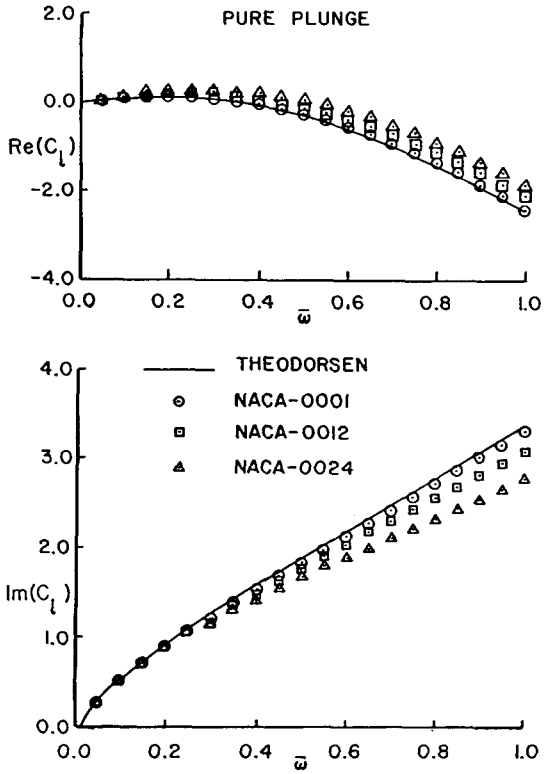

Figure 4. Effect of thickness on unsteady lift coefficient.

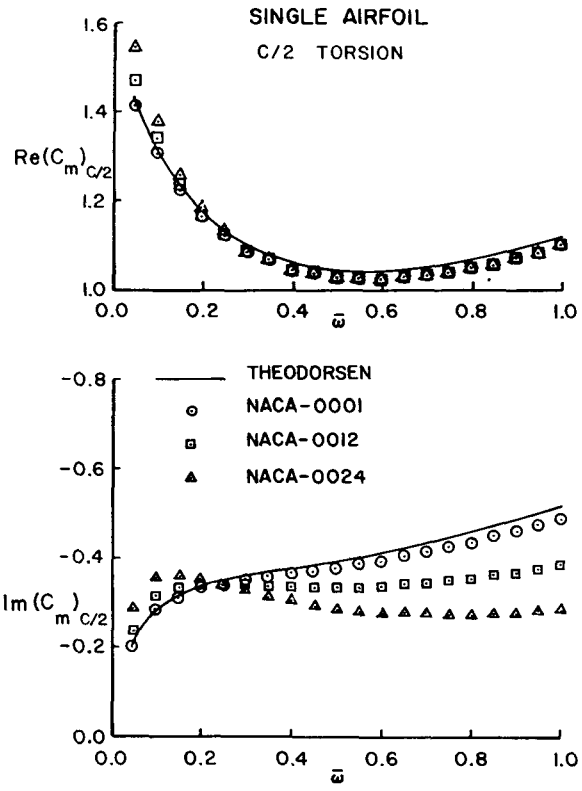

Figure 5. Effect of thickness on unsteady pitching moment coefficient.

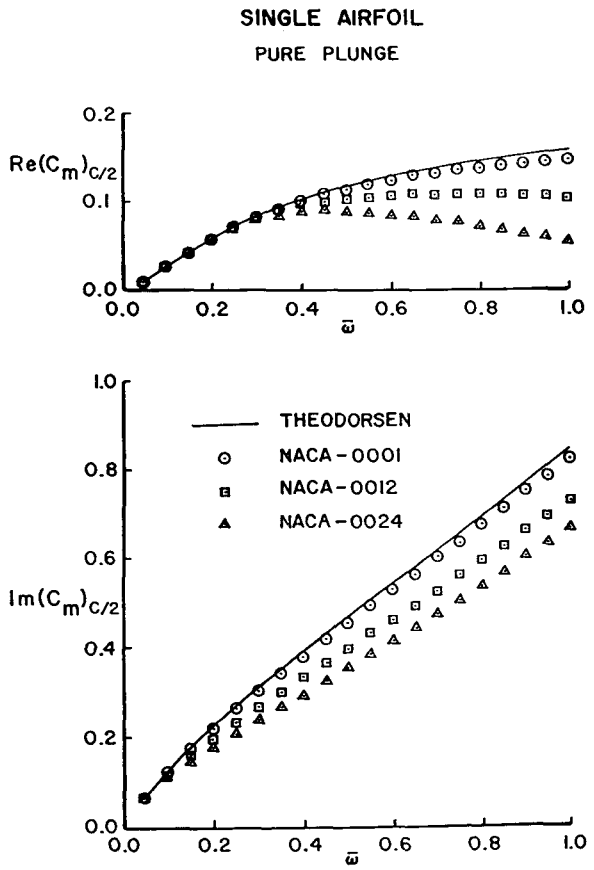

Figure 6. Effect of thickness on unsteady pitching moment coefficient.

differences in the flutter speed where the torsional mode is usually predominant. In these figures, the results are also presented for an airfoil with a 1% thickness. The purpose of the above exercise was two fold. In the first place, it was intended to demonstrate the stability of the vortex panel method even for extremely small values of this parameter. Numerical schemes based on source panel techniques usually fail in such cases. Secondly, comparison of the results for such an airfoil with those of the linear theory shows the ultimate convergence of the two methods as the thickness approaches zero. This fact is clearly evident throughout figures 3 through 6 . In addition, being assured of this fact, in considering multi-element cases where analytical results are no longer available, would allow substitution of small thickness results instead.

2. Multi-Element Unsteady Solution. Due to the absence of analytical solutions for these cases, a different approach was taken to verify the vortex panel results. Two computer codes were developed based on the linearized solutions of references 6 and 19. The first code employed the acceleration potential approach, while the second used the velocity potential formulation. Both techniques in their original form are for single element airfoils in subsonic flow. Compressibility effects were maintained in both codes in order to allow a thorough comparison of the two. Furthermore, both formulations were extended to include non-planer effects (i.e. multiple lifting surfaces). In both cases, the numerical solutions were obtained using standard collocation techniques. These two methods were compared, at low Mach

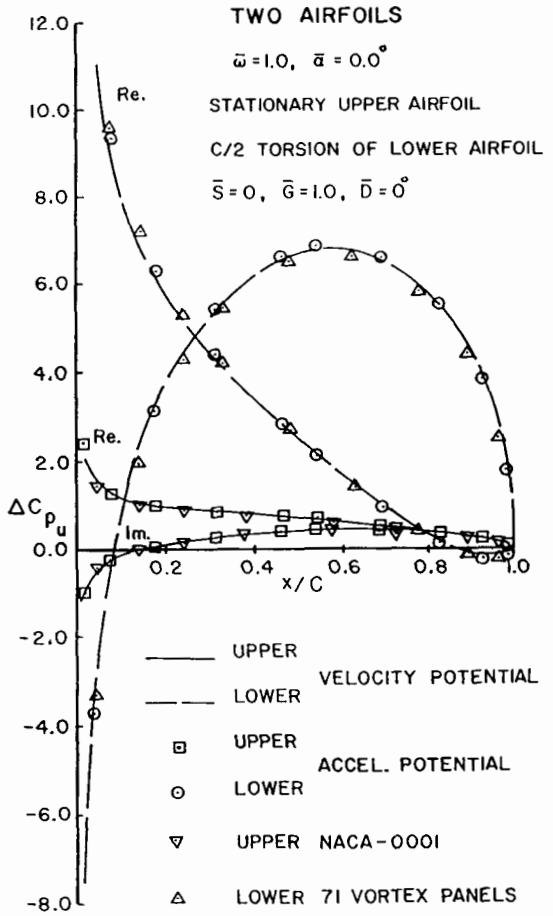

Figure 7. Comparison of the results of the three methods for two parallel airfoils.

numbers, with the vortex panel results. Figure 7 shows such a comparison. In this case, two parallel airfoils with no stagger and a gap of one chord length were used. The top airfoil was stationary while the lower airfoil executed harmonic torsion about its mid-chord. The purpose of this figure is three fold. First, it demonstrates the agreement between the two linearized solutions for a non-planer case. Secondly, it clearly verifies the vortex panel results approaching the linear solution with vanishing thickness. Finally, again it shows the stability of the vortex panel formulation in the presence of such small thickness ratios.

Having agreement among these three methods still was not considered sufficient proof of accuracy. Therefore, vortex panel results for two coupled airfoils were also compared with results of reference 7. Although the solution in this reference relied on acceleration potential formulation, the numerical scheme used there was considerably different. The results are presented in figure 8 . The basic geometry used for this case was the same as that of the previous one, except here the lower airfoil executed harmonic plunge. The excellent agreement between the two methods over a wide range of frequencies is quite evident from this figure. Therefore, from this point on the vortex panel method alone was used to explore the effects of thickness on the aerodynamic coefficients. Figure 9 shows the corresponding results for the pitching moment coefficient of the same geometry. Although the gap between the two

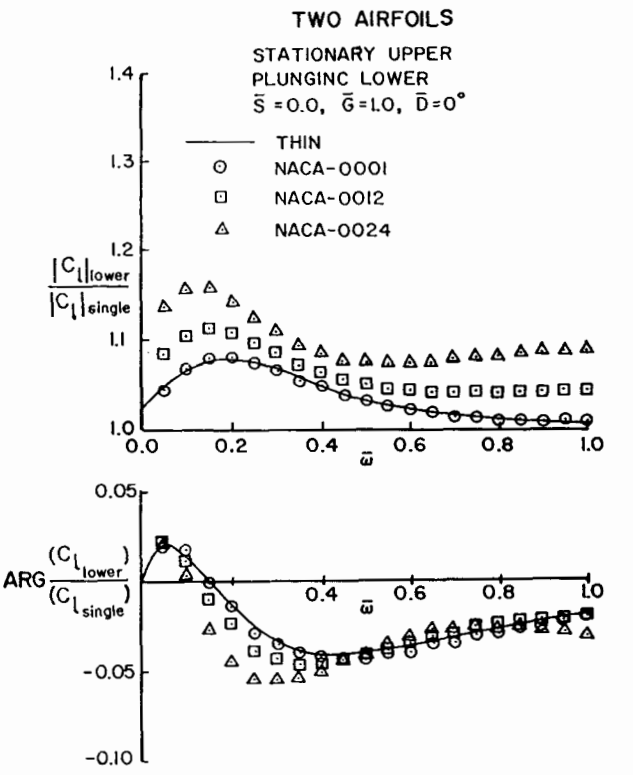

Figure 8. Effect of thickness on lift coefficient of two parallel airfoils.

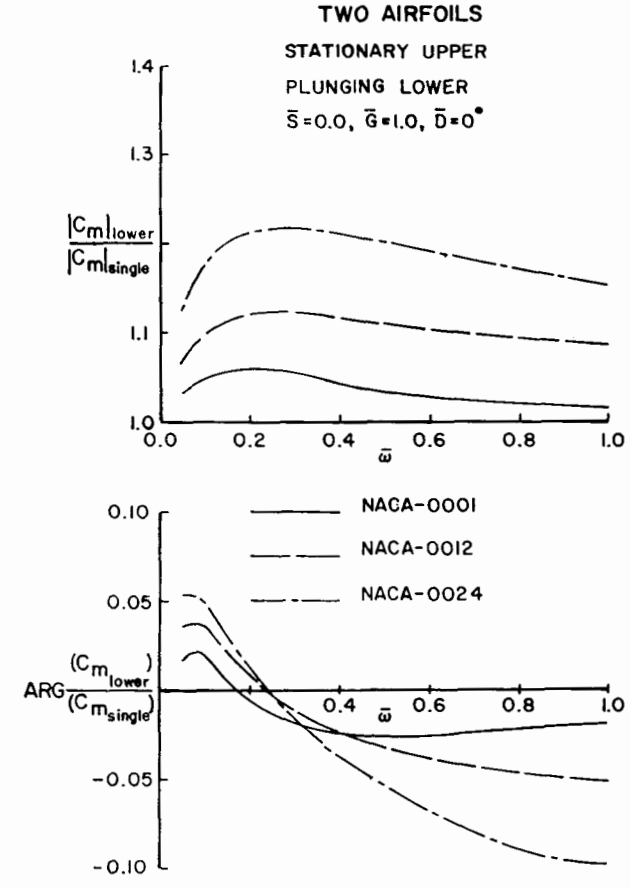

Figure 9. Effect of thickness on pitching moment coefficient of two parallel airfoils.

airfoils was moderately large, the pronounced effect of thickness on both the lift and the pitching moment coefficients is quite clear. Logically, these effects were expected to magnify with increased aerodynamic coupling in the presence of smaller gaps or slotted flaps. These trends are in complete accordance with the steady state solutions.

Figures 10 and 11 show the comparison of results for two 25.5% thick Joukowski sections, with gap and stagger of one half chord length each. The lower airfoil was stationary with the upper airfoil in harmonic torsion about its quarter chord point. The linear solution was first presented in reference 8 and the non-linear case was published in reference 10. Although these references contained the actual pressure coefficients, for the purpose of comparison with vortex panel results, they were converted to pressure differences. The good agreement among the three methods is quite evident in this figure. Also, noticeable is the smooth pressure distribution near the trailing edges that is predicted by the vortex panel method. However, large discrepancies in the imaginary part of the pressure on the lower airfoil are quite apparent. At this point, the exact cause is unknown, but Giesing (10) mentioned he had to modify the trailing edge shape of the airfoil to obtain an acceptable solution. The exact nature and magnitudes of those modifications were however omitted. Considering the robustness and accuracy of the vortex panel method which have been demonstrated so far, these authors tend to attribute the differences to those trailing edge modifications.

The final case considered here, was that of a strongly coupled slotted flap. For this purpose, an NACA-23012 airfoil was fitted with a 30% chord slotted flap deflected to 20 degrees. The main body of the airfoil was assumed stationary with the flap oscillating in torsion about its leading edge. It is noteworthy that this case cannot be modeled by any linear theory by any stretch of

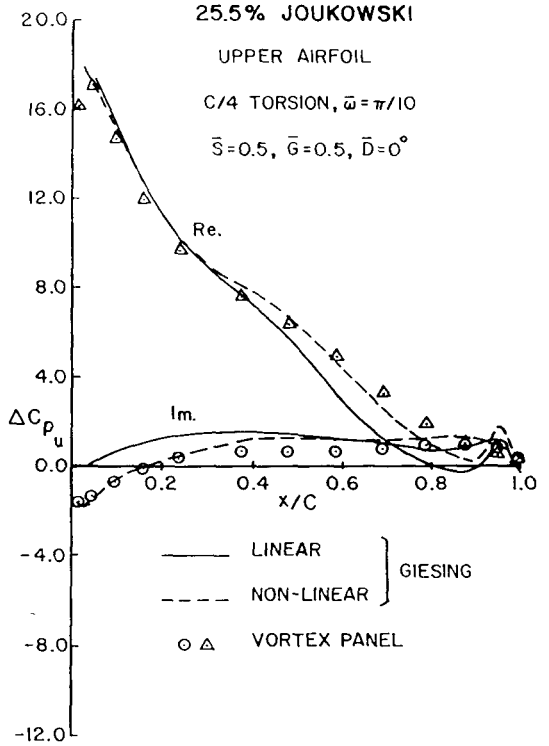

Figure 10. Unsteady pressure distribution on the upper airfoil

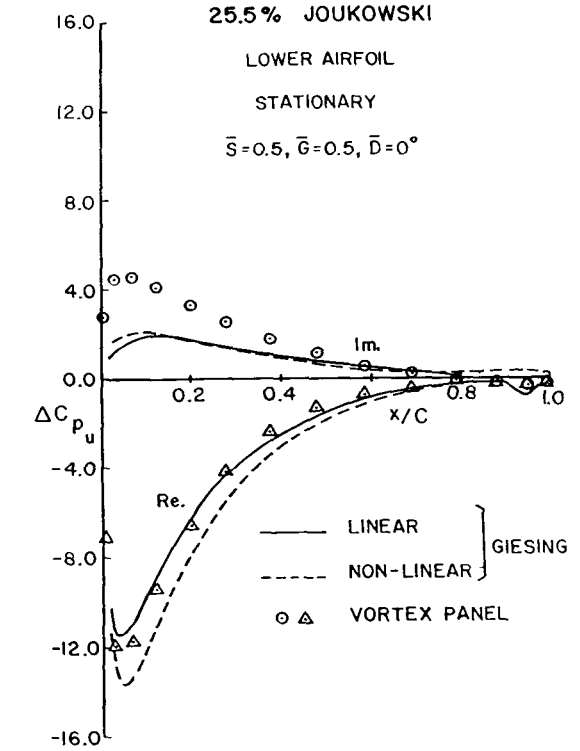

Figure 11. Unsteady pressure distribution on the lower airfoil

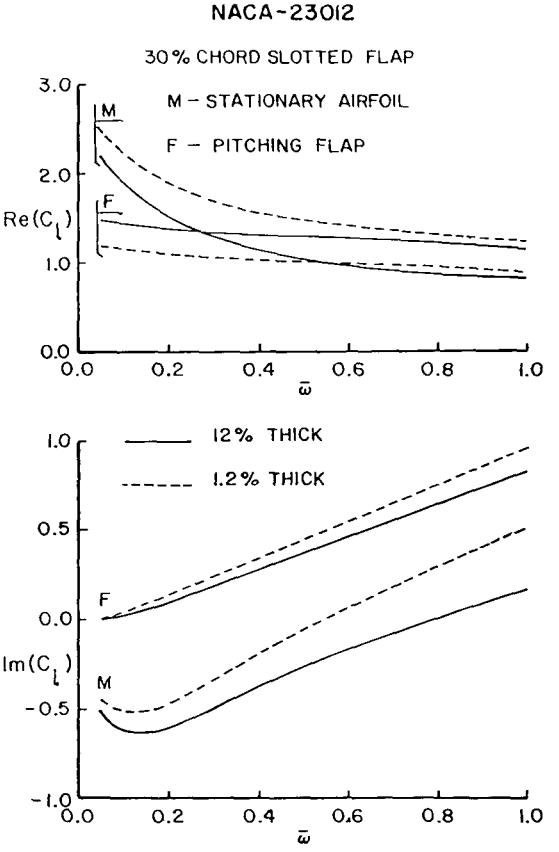

Figure 12. Effect of thickness on lift coefficient of an airfoil with a 30% chord slotted flap.

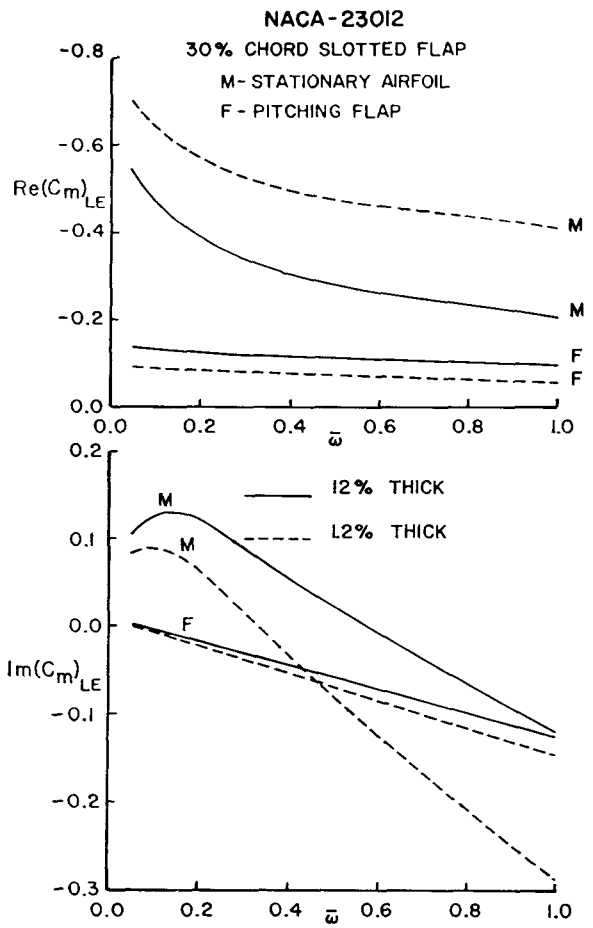

Figure 13. Effect of thickness on pitching moment coefficient of an airfoil with a 30% chord slotted flap.

imagination due to the large difference in the incidence angles of the airfoil and its flap. However, a model of the same geometry was constructed with the maximum thickness ratio reduced from 12% to 1.2%. Since the two models were identical in every respect, except for thickness ratio, any differences in pressures and aerodynamic forces had to be attributed to this parameter. The behavior of the lift and the pitching moment coefficients over a wide range of frequencies are presented in figures 12 and 13 . These figures show differences as large as 36% in the real part and 65% in the imaginary part of these parameters. These discrepancies are certainly large enough to demonstrate the need for including the effects of thickness in these calculations.

V. CONCLUSIONS

A vortex panel method was presented for solution of incompressible unsteady aerodynamic problems for lifting surfaces with finite thickness. The accuracy and robustness of the method was demonstrated through comparisons with the existing numerical data and independent test cases. Also, through numerous examples, the flexibility of this method was shown in handling different types of geometry.

Furthermore, the method was used to analyze the effects of airfoil thickness on aerodynamic coefficients of multi-element lifting systems. It was demonstrated that although the influence of thickness is negligible for single element airfoils, it can be profound for closely coupled airfoils and slotted flaps.

REFERENCES

1. Rokhsaz, K. "Aerodynamic Study of Dual Lifting Surfaces". M. S. Thesis, University of Missouri-Rolla, 1980.

2. Rokhsaz, K. and Selberg, B. P. "Disadvantages of Thin Airfoil Formulations for Closely Coupled Airfoils," Journal of Aircraft, Vol. 20, No. 6, pp 574-576, 1980.

3. Theodorsen, T. "General Theory of Aerodynamic Instability and the Mechanism of Flutter," NACA Report No. 496, 1935.

4. Hewsone-Browne, R. C. "The Oscillation of a Thick Airfoil in an Incompressible Flow," Quarterly Journal of Mechanics and Applied and Mathematics, Vol. XVI, Part I, 1963.

5. van de Vooren, A. I. and van de Vel, H. "Unsteady Profile Theory in Incompressible Flow," Archiwum Mechaniki Stosowanej, Vol. 3, No. 16, 1963.

6. Possio, C. "L'Azione Aerodynamica sul Profilo Oscillante in un Fluido Compressible a Velocita Isoponara," "L'Aerodynamica", t XVIII, fasc. 4, 1938. L'Aerodynamica, t XVIII, fasc. 4, 1938.

7. Grzedzinski, J. "Aerodynamic Interference in a System of Two Harmonically Oscillating Airfoils in an Incompressible Flow," Archiwum Mechaniki Stosowanej, Vol. 26, No. 3, 1974.

8. Giesing, J. P. "Nonlinear Two-Dimensional Unsteady Potential Flow with Lift," Journal of Aircraft, Vol. 5, No. 2, 1968.

9. Giesing, J. P. "Nonlinear Interaction of Two Lifting Bodies in Arbitrary Unsteady Motion," Transaction of ASME, Journal of Basic Engineering, Paper 68-FE-22, 1968.

10. Giesing, J. P. "Two-Dimensional Potential Flow Theory for Multiple Bodies in Small Amplitude Motion," AIAA Journal, Vol. 8, No. 11, 1968.

11. Hess, J. L. "The Problem of 3-D Lifting Potential Flow and its Solution by Means of Surface Singularity Distributions," Computer Methods in Applied Mechanics and Engineering, Vol. 4, 1974.

12. Hess, J. L. "The Use of Higher-Order Surface Singularity Distributions to Obtain Improved Potential Flow Solutions for Two- Dimensional Lifting Airfoils," Computer Methods in Applied Mechanics and Engineering, Vol. 5, 1975.

13. Hounjet, M. H. L. "ARSPNSC: A Method to Calculate Subsonic Steady and Unsteady Potential Flow about Complex Configurations," NLR-TR-86122-U, 1986.

14. Banerjee, P. K. and Butterfield, R. Boundary Element Methods in Engineering Science, United Kingdom, McGraw-Hill Book Company Limited, 1981.

15. Kuethe, A. M. and Chow, C. Y. Foundations of Aerodynamics, Fourth Edition New York, John Wiley & Sons, 1986.

16. Rokhsaz, K., "A Vortex Panel Method for Unsteady Aerodynamics of Multiple Lifting Surfaces with Thickness," Ph D Thesis, University of Missouri-Rolla, 1988.

17. Stevens, W. A., Goradia, S. H., and Braden, J. A. Mathematical Model for Two-Dimensional Multi-Component Airfoils in Viscous Flow," NASA CR-1843, 1971.

18. Moran, J. An Introduction to Theoretical and Computational Aerodynamics, New York, John Wiley & Sons, 1984.

19. Jones, W. P. and Moore, J. A. "Simplified Aerodynamic Theory of Oscillating Thin Surfaces in Subsonic Flow," AIAA Journal, Vol. 11, No. 9, 1973.